IECO International Journal Of Industrial Electronics Control and Optimization
Print ISSN: 3517-2645
Online ISSN: 3568-2645
Homepage: https://ieco.usb.ac.ir/

Study on Multi-Phase Boost Converters for Fuel Cell Application: Power Density and Reliability Analysis

Ghasem Rezazadeh | Hossein Bagherian Farahabadi

School of Electrical and Computer Engineering, College of Engineering, University of Tehran, Tehran, Iran.[1]
Northern Research Center for Science & Technology, Malek Ashtar University of Technology, Iran. [2]
Corresponding author's email: G.rezazadeh@ut.ac.ir

Article Info

Article type:
Research Article

Article history:
Received: 04-August-2025
Received in revised form: 06-December-2025
Accepted: 28-December-2025
Published online: 22-Dec-2026

Keywords:
Boost Converter,
Multi-phase,
Power Density,
Reliability.

ABSTRACT

This paper presents a new comprehensive study on multi-phase interleaved DC-DC boost converters for fuel cell power interface. High power density DC-DC converters are usually required due to the volumetric and gravimetric constraints in the various fuel cell power system applications. On the other hand, in sensitive applications such as vehicular systems, using a reliable converter is a critical feature. Therefore, different multi-phase configurations with various phase numbers are investigated to find the configuration with the highest power density and reliability. Boost converters with single, two, and four-phase configurations are designed with considerably low input current and output voltage ripples compatible with the fuel cell application. Their performance parameters (especially their power densities) are investigated using the analytical and simulation results. To discuss their reliability, a reliability analysis based on a mathematical model and a Markov diagram is employed to calculate the converters' expected load loss values. The novelty of this paper can be found in optimizing the aforementioned goal function by choosing the best multi-phase structure. In the end, among the considered configurations, the two-phase boost converter is selected to be used in fuel cell applications due to its superior performance in terms of power density and reliability. The selected boost configuration is implemented to extract the experimental results and verify the accuracy of the calculation and simulation results.

I. Introduction

Nowadays, the fossil fuel system is dwindling due to excessive utilization and burning of fossil fuels in the vehicular application, which leads to the emission of greenhouse gases [1], [2]. The fuel cell usually has a current source characteristic with low output voltage and high output current [3]. Therefore, to solve the mismatched problem of the voltage levels between the dynamic lower voltage of the fuel cell stack and the required constant higher voltage of the DC link, a DC-DC step-up converter should be used as the power electronic interface [4]-[6].

The boost converter is considered the most widely used converter in the fuel cell application [7]. Because this converter has three main features, including simple structure, high voltage gain (even without using transformers), and low input current ripple [8]. The research works on DC-DC boost converter in the fuel cell applications try to improve the converter performance in two different aspects: a) presenting an efficient converter model and control strategy [9]-[12] and b) improving the basis of the boost converter. Some research works in the second category are focused on enhancing the converter voltage gain using different methods such as cascading multiple basic boost converter cells [13], introducing the voltage multiplier [14], using switched capacitors [15], and series connection of the two modules at the output side [16]. Also, using the floating interleaved boost topology is a typical approach [17].

Using the interleaved multi-phase boost converters (with parallel connection of the modules) has some advantages, such as lower input current ripple, lower components' current stress, and more output power availability in case of fault occurrence [18]-[20]. These features make multi-phase interleaved boost converters appropriate in the fuel cell application because of the usually high current amplitude and low tolerable current ripple of the fuel cell. Therefore, in this paper, the multi-phase boost converters are used as a power interface between the fuel cell and the load.

Choosing the most suitable multi-phase configuration in the fuel cell application is a challenge studied in this paper. Choosing a converter topology with high power density is a critical goal in some applications, such as fuel cell hybrid vehicles. On the other hand, in some special applications such as vehicular systems, the selected topology should have high reliability to increase the converter's fault-tolerant capability [21]. Commonly, increasing the converter power density results in lower converter reliability and vice versa. Therefore, to achieve both high power density and reliability for the converter, the approach should be carefully implemented.

Many research efforts have been made on the reliability analysis of the DC-DC converter [22]-[24]. The reliability analysis starts with extracting the components' failure rate at different operating conditions. Then a proper reliability model could be used to make it clear how the components' failure rate is related to the converter reliability [25]-[27]. Using an analytical tool to illustrate the system states in terms of reliability, such as the Markov diagram, is a useful approach to calculating the converter reliability from the obtained model [28]-[30].

In this paper, single-phase, two-phase, and four-phase interleaved boost converters, which are three common interleaved structures, are studied for the fuel cell application. The converters are designed to have a very low current ripple that is compatible with the considered fuel cell. The new study aims to choose the multi-phase configuration with the highest power density and reliability. For this purpose, the converter components' volume and total expected load loss (ELL) are calculated analytically. The reliability analysis to compute ELL has been done using a proposed reliability model and a Markov diagram for the converters. To the knowledge of the authors, analysing the power density and reliability of these structures in the same time for finding the optimum structure with maximum goal function is not presented in the literature. This paper does not aim to present novel modeling or design methods, it should find the optimum structure with the highest reliability and power density. The novelty of this paper can be found in optimizing the aforementioned goal function by choosing the best multi-phase structure. The multi-phase converter with the highest power density and reliability is simulated and implemented, and the simulation and experimental results are presented to validate the analytical results.

TABLE I Electrical characteristics of the utilized fuel cell

Oper. point	Voltage (V)	Current (A)	Oper. point	Voltage (V)	Current (A)
1	41.7	0	7	31.5	150
2	37.6	25	8	31.2	175
3*	35.4	50	9	30.8	200
4	32.7	75	10	30.4	225
5	32.3	100	11	30	250
6	31.9	125	12	29.6	275

* Nominal operation point with rated values

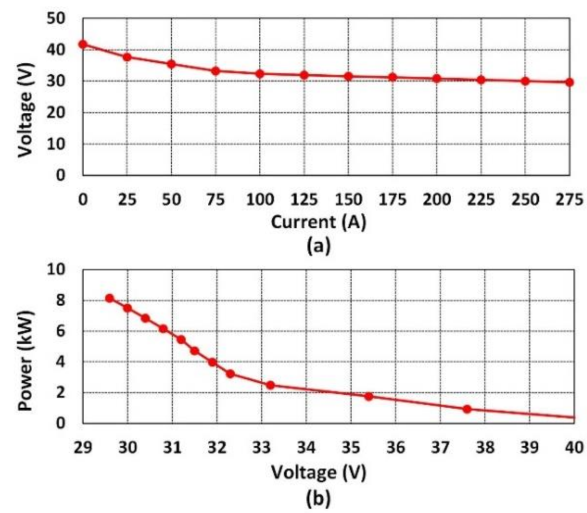

Fig. 1. Fuel cell (a) voltage-current and (b) power-voltage profiles.

TABLE II Electrical specifications of the required boost converter

Parameters	Symbol	Unit	Value
Rated input voltage	V_{i-fl}	V	35.4
Maximum input voltage	V_{i-nl}	V	41.7
Rated input current	I_{i-fl}	A	50
Rated input power	P_{i-fl}	W	1770
Maximum input current ripple	ΔI_{i-max}	A	0.5
Rated output voltage	V_o	V	72
Rated output power	P_o	W	1600
Rated output current	I_o	A	22.2
Maximum output voltage ripple	ΔV_{o-max}	V	0.4
Switching frequency	f_s	kHz	25

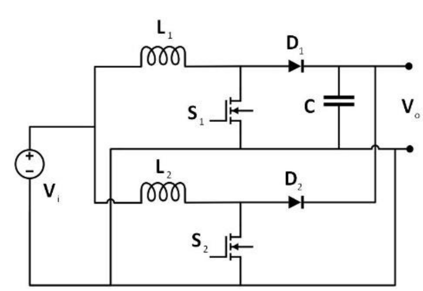

Fig. 2. Two-phase boost converter.

II. Supply power and converter specifications

The fuel cell is a power source with direct voltage and current. Technically, the characteristics of the fuel cell include parameters related to its electrical behaviour, such as rated input voltage, minimum operating voltage, maximum

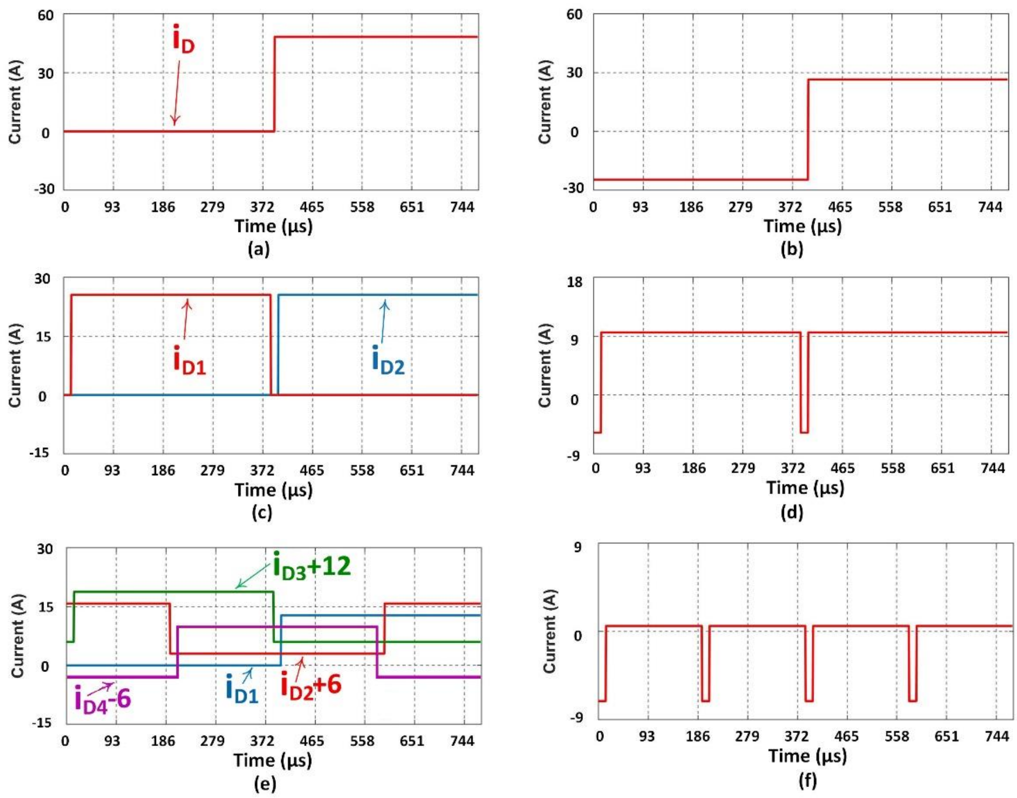

Fig. 3. Diode and capacitor currents for different designed multi-phase boost converters: (a) diode and (b) capacitor currents for single-phase, (c) diode and (d) capacitor currents for two-phase, and (e) diode and (f) capacitor currents for four-phase.

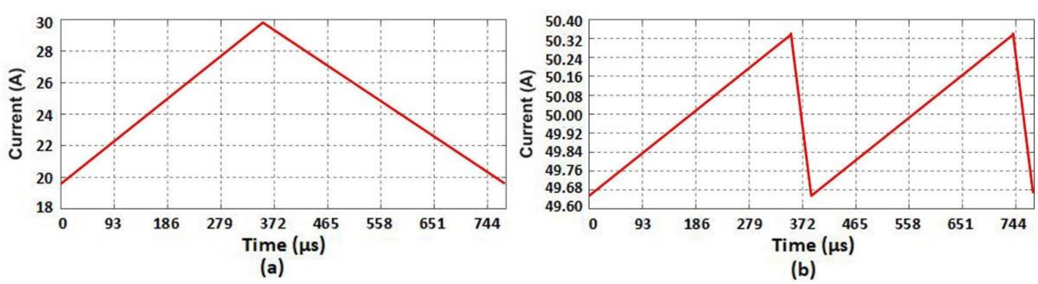

Fig. 4. The two-phase boost converter currents, (a) The phase input current, (b) The total input current.

operating voltage, rated power, and rated supply current. With the studies performed on the existing power supply system, the electrical parameters of the fuel cell are extracted and shown in Table I.

According to the reported fuel cell characteristics, the nominal input power of the designed boost converter should be equal to 1770 W at 35.4 V. Another critical fact related to the fuel cell behaviour is the voltage variation by changing the electrical load value. Using the presented fuel cell, the converter input voltage varies from 41.7 V to 35.4 V from no-load to full-load conditions, respectively. To show the load-dependent behaviour of the fuel cell, its voltage-current and power-voltage profiles are shown in Fig. 1.

The reported fuel cell has a specific feature, which is its sensitivity to the output current ripple. To protect the fuel cell, the input current ripple of the converter must be less than one percent. Based on the aforementioned facts about the considered fuel cell as the supply voltage, the required boost converter specifications are reported in Table II.

III. Multi-phase boost

In multi-phase structures, parallel power flow paths are used with a converter in each path. Fig. 2 shows the structure of a two-phase boost converter. The current passing from the converter input to output is divided between the converter phases, which reduces the nominal currents of the components used in each phase. In other words, using a multi-phase structure increases the number of elements required and decreases their nominal values. This feature simplifies the selection of converter components for a specified required power, especially in high-power applications.

However, the multi-phase structure has another critical advantage, and that is a significant reduction in the required capacitor and inductance amounts to have an acceptable input current and output voltage ripples. The utilized phase shift angle between different phases is the main tool to achieve this feature. In the symmetrical multi-phase structures, there is a phase difference of 360º/n degrees between different stages, where n indicates the number of phases. For example, in the two-phase structure shown in Fig. 2, the switching period of the second phase switch (S_2) starts 180 degrees after that of the switch S_1. In this case, when S_1 in the first phase is on and the power transmission path from input to output is interrupted, S_2 can be off, and the power can be transmitted from input to output in the second phase of the converter. This feature reduces the required capacitor amount to supply the output current when the phase switch is on.

In this paper, single-phase, two-phase, and four-phase boost converters for the power interface of the fuel cell supply are investigated and compared with each other. Therefore, in this section, the operation principles of these three converters are examined. It should be noted that due to the sensitivity of the fuel cell to the output current ripple, the converters will operate in continuous conduction mode (CCM) so that their input current ripple is minimum.

It should be noted that the capacitor and inductance volumes are the two very important factors in determining the converter size. Therefore, the effect of the required output voltage ripple and the converter structure on the capacitor value and consequently, its volume is studied. Then, the same investigation to find the input current ripple and the converter structure influences on the inductance volume is presented.

A. Output capacitor of multi-phase boost

In multi-phase boost converters, the capacitor current can be calculated as [22]:

$$I_c = \sum_{j=1}^{n} i_{d-j} - I_o \tag{1}$$

where i_{d-j} is the diode current in phase j and I_o is the average output current of the converter. In Fig. 3, the total capacitor current and the diode current of each converter phase are presented for single, two, and four-phase converters. After calculating the area below the capacitor current waveform from zero to zero (ΔQ), the required amount of capacitor can be described as [22]:

$$C_{out} = \frac{\Delta Q}{\Delta V_0} = \frac{\Delta Q}{Allowable\ voltage\ ripple = 0.006 \times V_0} \tag{2}$$

It should be noted that the load change transient such as load steps are not considered in this paper.

B. Current ripple

The input current ripple for each phase of the multi-phase boost converter can be calculated as follows [4]:

$$L = \frac{V_i D T_s}{\Delta I_L} \tag{3}$$

where D is the switch duty cycle and T_s is the switching period. The fuel cell current is equal to the sum of the inductance currents of the phases. Due to the phase shift angle between the inductance currents of the phases, the input current ripple is much lower than the current ripple of each inductance. For example, Fig. 4 shows the phase input current and the total input current of a two-phase boost converter.

IV. Converter size

Using the above-mentioned design procedure, single-phase, two-phase, and four-phase boost converters are designed, and the required component values are presented in Table III. It should be noted that the well-known procedure of designing a multi-phase boost converter is not presented in this paper for the sake of brevity. The total volumes of the designed components for the multi-phase boost converters are reported in Table IV.

TABLE III Design results for the required boost converter

Component	Part	N	Value	Voltage	Current
A. Single-phase boost converter					
Output cap.	Electrolyte	9	100 µF	100 V	-
Output cap.	Electrolyte	2	47 µF	100 V	-
Input ind.	-	1	1.47 mH	-	60 A
Switch	IRFP4227PBF	1	-	200 V(1)	46 A(2)
Diode	MBR40100CT	1	-	100 V(3)	40 A(4)
B. Two-phase boost converter					
Output cap.	Electrolyte	2	100 µF	100 V	-
Output cap.	Electrolyte	2	47 µF	100 V	-
Input ind.	-	2	100 µH	-	30 A
Switch	IRFP4227PBF	2	-	200 V(1)	46 A(2)
Diode	MBR20150PT	2	-	150 V(3)	20 A(4)
C. Four-phase boost converter					
Output cap.	Electrolyte	1	100 µF	100 V	-
Output cap.	Electrolyte	2	47 µF	100 V	-
Input ind.	-	4	60 µH	-	15 A
Switch	IRFP240	4	-	200 V(1)	12 A(2)
Diode	MBR20150PT	4	-	150 V(3)	20 A(4)

(1) Switch drain-source minimum breakdown voltage
(2) Switch drain-source continuous current @ 100ºC
(3) Diode peak repetitive reverse voltage
(4) Diode forward current @ 100ºC

The design results clearly show that the two-phase and four-phase configurations use 81.1% and 77.6% less required component volumes compared to the single-phase configuration, respectively. Therefore, from the highest to the lowest power density, the considered boost converter can be listed as the two-phase, four-phase, and single-phase configurations. Considering the aforementioned results, using the multi-phase structure for the required boost

TABLE IV Total volume of the designed boost converters

Converter type	Component	Volume (cm^3)	Component	Volume (cm^3)
Single phase	Output cap.	51.1	Switches	3.1
	Input ind.	295.5	Diodes	1.4
	Converter total component volume: 351.1 cm^3			
Two phase	Output cap.	16.8	Switches	6.2
	Input ind.	40.2	Diodes	2.9
	Converter total component volume: 66.1 cm^3			
Four phase	Output cap.	11.9	Switches	12.5
	Input ind.	48.2	Diodes	5.8
	Converter total component volume: 78.4 cm^3			

converter significantly reduces the converter volume and consequently increases the converter power density. The reliability analysis is followed to select the best multi-phase structure among the two-phase and four-phase ones.

V. Reliability analysis

First, before starting the reliability analysis, the utilized analysis assumption can be described as:

- Without receiving a proper performance from any power components of each parallel path, the transmitting power in that phase is zero. In other words, the component failure in each phase will result in phase failure.
- If the inductor current ripple in each phase exceeds its allowable value, the protection switch corresponding to this phenomenon will trip, and the whole system will be turned off. This phenomenon is due to the low ability of the reported fuel cell to withstand the current ripple.
- In the multi-phase structure, in case of a phase failure, the other phases can continue to operate normally.
- The control system of the multi-phase structure is integrated and the fault occurrence in it disrupts the whole power delivery capability of the system.

A. Reliability analysis principles

The reliability function (probability of being healthy) is an indicator for determining the reliability of the system in terms of time, which is defined as the number of healthy units at time *t* divided by the number of units [25]:

$$R(t) = \frac{N_s(t)}{N_o} \tag{4}$$

The system failure probability function is also defined as the number of the failed units to the total number of the units examined [25]:

$$Q(t) = \frac{N_f(t)}{N_o} \tag{5}$$

The relationship between the reliability function and the failure probability function is as follows [25]:

$$R(t) + Q(t) = 1 \tag{6}$$

The failure rate of each element is a function of time, which is defined as the number of failures in the defined period divided by the number of elements exposed to failure [26]:

$$\lambda(t) = \frac{Number\ of\ failures\ per\ unit\ time}{Number\ of\ components\ exposd\ to\ failure} \tag{7}$$

According to the definitions, the relationship between the reliability function and the failure rate will be as follows [28]:

$$\lambda(t) = \frac{1}{N_s(t)} \cdot \frac{dN_f(t)}{dt} = \frac{-1}{R(t)} \cdot \frac{dR(t)}{dt} \rightarrow R(t) = e^{-\int \lambda(t)dt} \tag{8}$$

In many operational examples, the value of the failure rate function has a constant value over the component useful lifetime. By inserting the value of the failure rate, we will have [24]:

$$R(t) = e^{-\lambda t} \tag{9}$$

The component manufacturer can report the component failure rate by performing some reliability tests on it.

B. Component failure rate

In this section, explanations will be provided on how to calculate the failure rate of the elements used in the converter. Most systems have three parts of reliability [25]:

- Software reliability
- Hardware reliability
- Human reliability

Generally, in the reliability evaluation of power electronics systems, hardware reliability is examined and introduced as the system reliability. The most important factor determining the system's reliability is the failure rate. System failure is examined in three different periods [25]:

- Initial failure: At this time, which generally includes the construction conditions, the failure rate decreases over time.
- Lifetime failure: During the useful life of the system, the failure rate of the system can be assumed to be constant.
- Aging failure: After the useful life of the system, the failure rate of the system increases over time.

Here, the system is examined only in its useful lifetime. From now on, the reports on the failure rate of components mean their constant failure rate during their useful lifetime.

This section aims at obtaining the failure rate of the power switch, diode, capacitor, and inductance to extract the hardware reliability of the converter. To obtain the failure rate of each component, a concept called the base failure rate of that component is used. The MIL-HDBK-217 handbook states that the base failure rate can be calculated based on the following formula for components [27]:

$$\lambda_b = A \times \exp\left(\frac{N_T}{273 + T + (\Delta T)S}\right) \times \exp\left(\frac{273 + T + (\Delta T)S}{T_M}\right) \tag{10}$$

In this equation, A is the proportionality coefficient. N_T, T_M and P are the shape and structure-related coefficients. T

represents the temperature and ΔT indicates the maximum allowable temperature difference between no current and full current conditions. S is a stress-related coefficient. For some products, the base failure rate is provided by the manufacturer. By having the basic failure rate value in hand, the failure rate value of each part can be obtained by using the following equations [25]-[27].

- *Switch failure rate:*

$$\lambda_{SW} = \lambda_{b-SW}\pi_T\pi_A\pi_Q\pi_E \quad (11)$$

The coefficients used after the base failure rate, from left to right, are related to temperature, application, product quality, and environmental conditions [25].

- *Diode failure rate:*

$$\lambda_D = \lambda_{b-D}\pi_T\pi_C\pi_S\pi_Q\pi_E \quad (12)$$

In this regard, π_C is the contact structure coefficient and π_S is the stress coefficient [25].

TABLE V Failure rate of designed components [25]

Component	Part	Value	Pack.	Failure rate (1/hour)
Capacitor	Electrolyte	100 µF	-	10^{-7}
Capacitor	Electrolyte	47 µF	-	10^{-7}
Inductance	-	60 µH	-	3.8×10^{-8}
Inductance	-	100 µH	-	3.8×10^{-8}
Inductance	-	1.47 mH	-	3.8×10^{-8}
Switch	IRFP4227PBF	-	TO247	3.8×10^{-9}
Diode	MBR20150PT	-	TO-3P	1.5×10^{-9}

- *Capacitor failure rate:*

$$\lambda_{Cap} = \lambda_{b-Cap}\pi_{CV}\pi_Q\pi_E \quad (13)$$

Where π_{CV} is the capacitor value coefficient [25].

- *Inductor failure rate:*

$$\lambda_{Ind} = \lambda_{b-Ind}\pi_C\pi_Q\pi_E \quad (14)$$

Each of the above-mentioned coefficients has an experimental formula or a lookup table to be calculated. In this paper, to simplify the process of calculating reliability, we consider all experimental coefficients as one. In other words, the effect of operation and production conditions on the components' failure rates is ignored to simplify the reliability analysis procedure, which is already complicated enough. The failure rates for the components of the designed boost converter are reported in Table V.

C. Reliability modeling

Considering the operation principle of the multi-phase boost converters and the utilized assumptions for reliability analysis, the reliability model can be described as:

- The components used in each phase of the boost converter are modelled in a reliability equivalent circuit and placed next to each other in series because the failure of any phase component means that phase is out of the power delivery.
- The different phases of the boost converters are modelled in parallel in the equivalent circuit. The reason is the independence of the power delivery process in each phase compared to the other ones.
- If the input current ripple exceeds 0.5 A, the entire system will shut down.

The equivalent circuit of the system is shown in Fig.5.

Due to the series connection of the components in each phase, the phase failure rate is equal to the sum of all components' failure rates in that phase:

$$\lambda_i = \lambda_{D-i} + \lambda_{SW-i} + \lambda_{Ind-i} + \lambda_{Cap-i} \quad (15)$$

The reliability function of each phase is defined as follows:

$$R_i(t) = e^{-\lambda_i t} = e^{-(\lambda_{D-i}+\lambda_{SW-i}+\lambda_{Ind-i}+\lambda_{Cap-i})t} \quad (16)$$

Now, the failure rate and reliability function of the phases are defined. To continue the reliability calculation process of the system, it is not possible to simply consider the different phases in parallel and obtain the reliability function of the whole system. Due to the presence of the input current ripple constraint, the different phases are conditionally parallel. To obtain the relation between the failure rates of the phases and the system, two different operating conditions are examined using the Markov diagram.

- Without input current ripple protection:

In this case, due to the fact that the input current ripple protection is not utilized, the converter continues to work when each phase fails; however, it provides less output power than the nominal operating condition. Therefore, there will be three modes in the Markov diagram: healthy (converter works perfectly), partial fail (some of the phases are lost), and fail (the whole converter does not transfer power and it is not functional) [31]. The Markov diagrams for the reliability analysis of the multi-phase boost converters are shown in Fig. 6 [32]. As can be seen, the three modes are defined in this figure. In the healthy and fault modes, there is only one state considering the basic definition of these modes [31]. The partial fault mode could contain multiple states, where at least one of the phases is lost in these states, but not all of them [32]. In the presented Markov diagrams, the related failure rates for transferring from one to another state are shown. This way, the Markov diagram can show the probability of transferring from one state to another [31]. It should be noted that each phase is considered as a unit. Assuming that the units are similar, the failure rates of all units are equal. According to the Markov diagrams, the system failure rates for the multi-phase converters without using input current ripple protection can be expressed as follows for the single-phase converter:

$$\begin{gathered} All\ possible\ states\ for\ n\ phase: \big(R(t) + Q(t)\big)^n \\ 1\ phase: \begin{cases} 1\ up \rightarrow R_1(t) = e^{-\lambda_{1s}t} \\ no\ up \rightarrow Q(t) = 1 - e^{-\lambda_{1s}t} \end{cases} \end{gathered} \quad (17)$$

For the two-phase converter, we will have:

$$2\ phase: \begin{cases} 2\ up \rightarrow R_2(t) = e^{-2\lambda_{2s}t} \\ 1\ up \rightarrow R_1(t) = 2e^{-\lambda_{2s}t}(1 - e^{-\lambda_{2s}t}) \\ no\ up \rightarrow Q(t) = (1 - e^{-\lambda_{2s}t})^2 \end{cases} \quad (18)$$

where, λ_{s1}, λ_{s2}, and λ_{s4} are the failure rates of one phase in single-phase, two-phase, and four-phase structures, respectively. It should be noted that the probability of complete failure in the four-phase converter is lower than in the other ones and this configuration has the highest availability feature. On the other hand, the single-phase boost converter has the highest probability of remaining completely healthy.

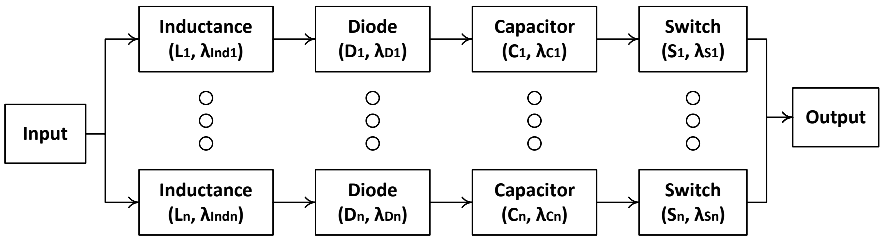

Fig. 5. . Equivalent circuit for the reliability model of multi-phase Boost converter.

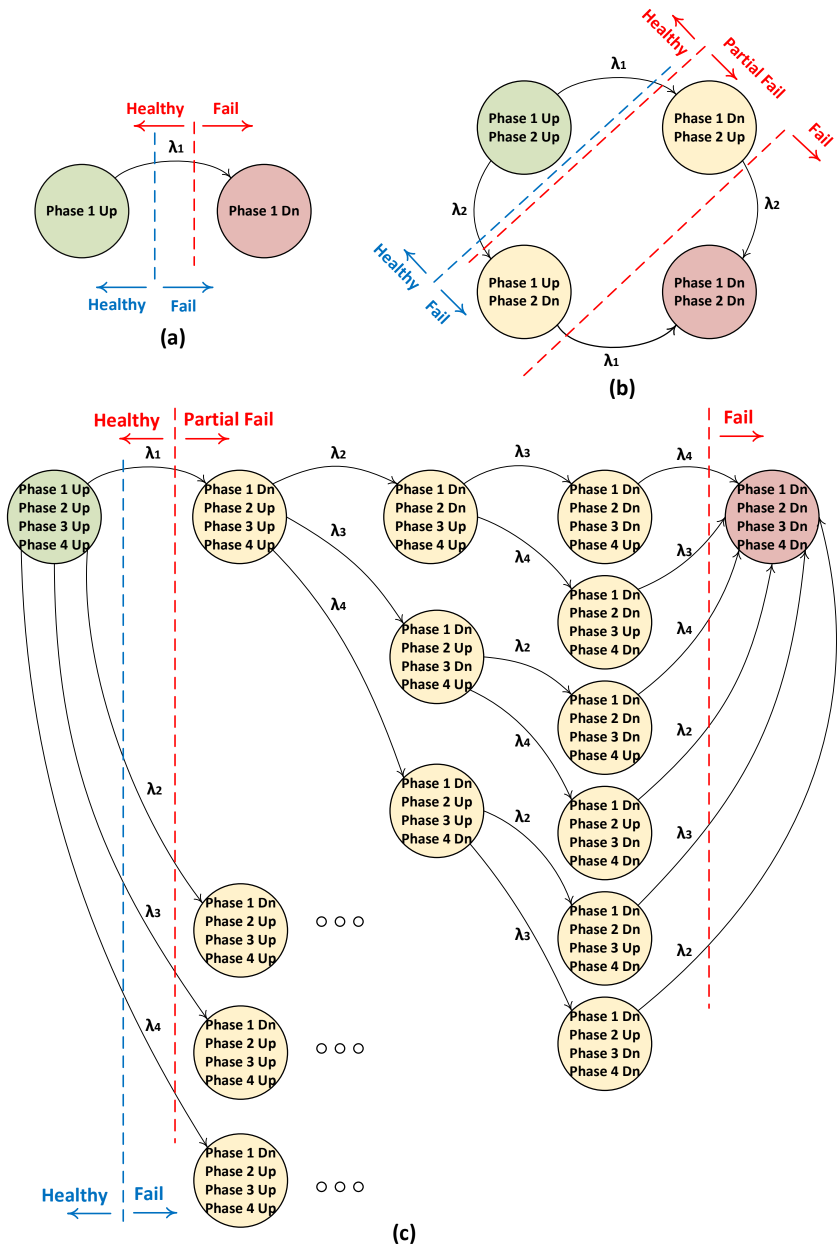

Fig. 6. Markov diagrams for the reliability analysis of the multi-phase boost converters: (a) single-phase, (b) two-phase, and (c) four-phase configurations. Modes for Case 1 (without input current ripple protection) are defined in red and modes for Case 2 (with input current ripple protection) are defined in blue.

At the end, the system failure rates for the four-phase converter can be described as:

$$2\ phase: \begin{cases} 4\ up \rightarrow R_4(t) = e^{-4\lambda_{4s}t} \\ 3\ up \rightarrow R_3(t) = 4e^{-3\lambda_{4s}t}\left(1 - e^{-\lambda_{4s}t}\right) \\ 2\ up \rightarrow R_2(t) = 6e^{-2\lambda_{4s}t}\left(1 - e^{-\lambda_{4s}t}\right)^2 \\ 1\ up \rightarrow R_1(t) = 4e^{-\lambda_{4s}t}\left(1 - e^{-\lambda_{4s}t}\right)^3 \\ no\ up \rightarrow Q(t) = \left(1 - e^{-\lambda_{4s}t}\right)^4 \end{cases} \quad (19)$$

An appropriate criterion for examining and comparing the reliability of two systems with the ability to supply power partially (such as multi-phase structures) is the Expected Load Loss (ELL). This quantity is the sum of the product of the power loss and the probability of losing it. This parameter can be expressed in terms of time [25]:

$$ELL|_{t=t_0} = \sum_i P_{loss-i} R_i(t = t_0) \quad (20)$$

The ELL for the single-phase converter can be calculated as follows:

$$ELL_{1s}(t) = P_{out}\left(1 - e^{-\lambda_{1s}t}\right) \quad (21)$$

The ELL for two-phase is:

$$ELL_{2s}(t) = \frac{P_{out}}{2} 2e^{-\lambda_{2s}t}\left(1 - e^{-\lambda_{2s}t}\right) + P_{out}\left(1 - e^{-\lambda_{2s}t}\right)^2 \quad (22)$$

And finally for four-phase converter, we will have:

$$ELL_{4s}(t) = \frac{P_{out}}{4} 4e^{-3\lambda_{4s}t}\left(1 - e^{-\lambda_{4s}t}\right) + \frac{P_{out}}{2} 6 e^{-2\lambda_{4s}t}\left(1 - e^{-\lambda_{4s}t}\right)^2 + \frac{3P_{out}}{4} 4e^{-\lambda_{4s}t} \left(1 - e^{-\lambda_{4s}t}\right)^3 + P_{out}\left(1 - e^{-\lambda_{4s}t}\right)^4 \quad (23)$$

- With input current ripple protection:

In this case, there is a protection circuit that shuts down the converter if the input current ripple exceeds 0.5 A. Thus, although the converter may provide part of the output power in case of phase failure occurrence, the protection system turns off the converter. In other words, if each phase fails, the whole converter fails. The Markov diagram for this scenario is shown in Fig. 6. According to the presented diagram, the reliability function for the single-phase can be calculated as follows:

$$1\ phase: \begin{cases} system\ up \rightarrow R(t) = e^{-\lambda_{1s}t} \\ system\ down \rightarrow Q(t) = 1 - e^{-\lambda_{1s}t} \end{cases} \quad (24)$$

The same can be expressed for two-phase:

$$2\ phase: \begin{cases} system\ up \rightarrow R(t) = e^{-2\lambda_{2s}t} \\ system\ down \rightarrow Q(t) = 2e^{-2\lambda_{2s}t} \\ \left(1 - e^{-\lambda_{2s}t}\right) + \left(1 - e^{-\lambda_{2s}t}\right)^2 \end{cases} \quad (25)$$

For the four-phase, we will have:

$$4\ phase: \begin{cases} system\ up \rightarrow R(t) = e^{-4\lambda_{4s}t} \\ system\ down \rightarrow Q(t) = 4e^{-3\lambda_{4s}t} \\ \left(1 - e^{-\lambda_{4s}t}\right) + 6e^{-2\lambda_{4s}t}\left(1 - e^{-\lambda_{4s}t}\right)^2 \\ +4e^{-\lambda_{4s}t}\left(1 - e^{-\lambda_{4s}t}\right)^3 + \left(1 - e^{-\lambda_{4s}t}\right)^4 \end{cases} \quad (26)$$

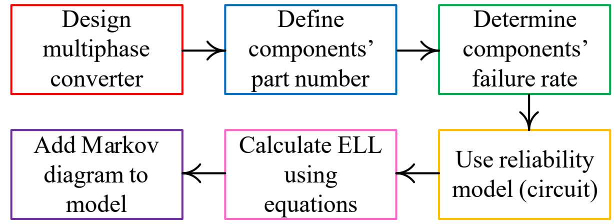

Fig. 7. ELL calculation procedure

TABLE VI Expected load loss after one million hours for different multi-phase converters

Converter	Input current ripple protection	ELL
Single-phase	Considered	$0.1306\times P_{out}$
	Not considered	$0.1306\times P_{out}$
Two-phase	Considered	$0.2271\times P_{out}$
	Not considered	$0.1306\times P_{out}$
Four-phase	Considered	$0.3434\times P_{out}$
	Not considered	$0.1306\times P_{out}$

TABLE VII Expected load loss after one million hours for different multi-phase converters

Phase number	Input current ripple protection	ELL (pu)*	Volume (pu)**	Objective function
1	Considered	0.1306	1	0.1306
2	Considered	0.2271	0.188	0.0427
4	Considered	0.3434	0.233	0.0800

* normalized considering the rated output power
** normalized considering the single-phase volume

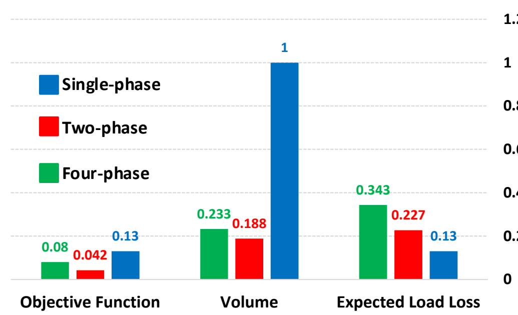

Fig. 8. ELL and volume calculation result

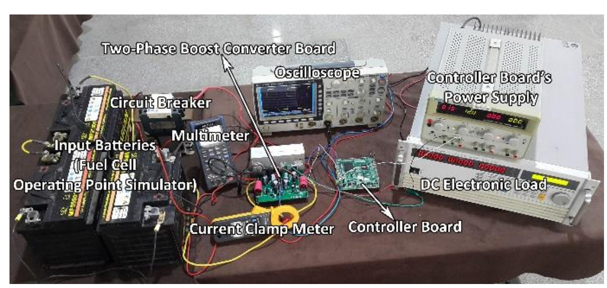

Fig. 9. Utilized test setup for the implemented two-phase boost converter.

Obviously, in this situation where the input current protection system is functional, the four-phase converter is not suitable in terms of reliability because the failure in any component results in phase failure, which is equivalent to not having access to the output power. On the other hand, the probability of any failure occurrence in the four-phase converter is higher than that in other converters, because of its larger number of utilized components. In the presence of the input current ripple protection system, the single-phase converter is more reliable due to the small number of

components used in it. The expected load loss for the single-phase case is obtained as follows:

$$ELL_{1s}(t) = P_{out}(1 - e^{-\lambda_{1s}t}) \quad (27)$$

For the two-phase, we will have:

$$ELL_{2s}(t) = P_{out}\left(e^{-\lambda_{2s}t}\left(1 - e^{-\lambda_{2s}t}\right) + \left(1 - e^{-\lambda_{2s}t}\right)^2\right) \quad (28)$$

And the ELL for the four-phase is:

$$ELL_{4s}(t) = P_{out}\left(e^{-3\lambda_{4s}t}\left(1 - e^{-\lambda_{4s}t}\right) + e^{-2\lambda_{4s}t}\left(1 - e^{-\lambda_{4s}t}\right)^2 + e^{-\lambda_{4s}t}\left(1 - e^{-\lambda_{4s}t}\right)^3 + \left(1 - e^{-\lambda_{4s}t}\right)^4\right) \quad (29)$$

In this step of the reliability analysis, the expected load loss values (after one million hours) for different multi-phase converters are calculated (Fig. 7) in two modes with and without input current ripple protection (Table VI).

As was expected, the single-phase structure has the best performance considering the ELL value. However, the four-phase (especially when the protection system exists) has the highest ELL value, which indicates its low reliability. It should be noted that even though the four-phase structure has the lowest reliability, it has the highest availability.

VI. Comparison of multi-phase configurations

The selection of the optimal phase number will be done according to an objective function consisting of the expected load loss and the required volume of the converter:

$$Objective\ function = ELL \times Volume \quad (30)$$

It should be noted that the converter volume is defined as the sum of the main components' volumes (power switch, diode, inductance, and capacitor) to avoid the complexity of considering the components' arrangement in the actual circuit. On the other hand, the worst-case scenario for the converters' reliability is taken into account, where the input current ripple protection exists. The multi-phase converter with the lowest objective function value will be selected as the best option for use in fuel cell applications.

According to the results reported in Table VII and Fig. 8, the single-phase structure is more reliable than the other two options, and the two-phase structure is the best option in terms of volume in comparison with the other ones. In the end, the two-phase structure has the lowest objective function, thus, the two-phase structure is selected as the desired option. It should be noted that the results presented in Table VII are normalized using the rated output power as the normalization base for ELL and the highest converter's volume (single-phase's volume) as the normalization base for volume.

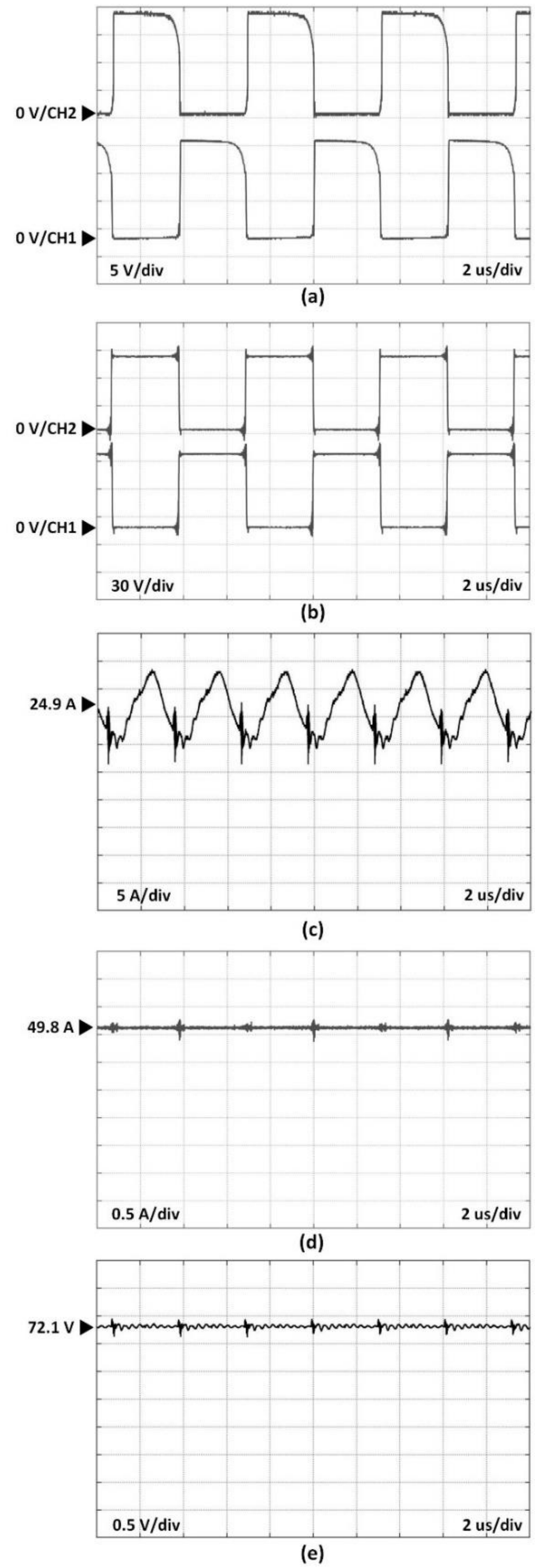

Fig. 10. Experimental results for the implemented two-phase boost converter: (a) gate-source voltage for both switches, (b) drain-source voltage for both switches, (c) phase input current (d) converter input current, (e) output voltage.

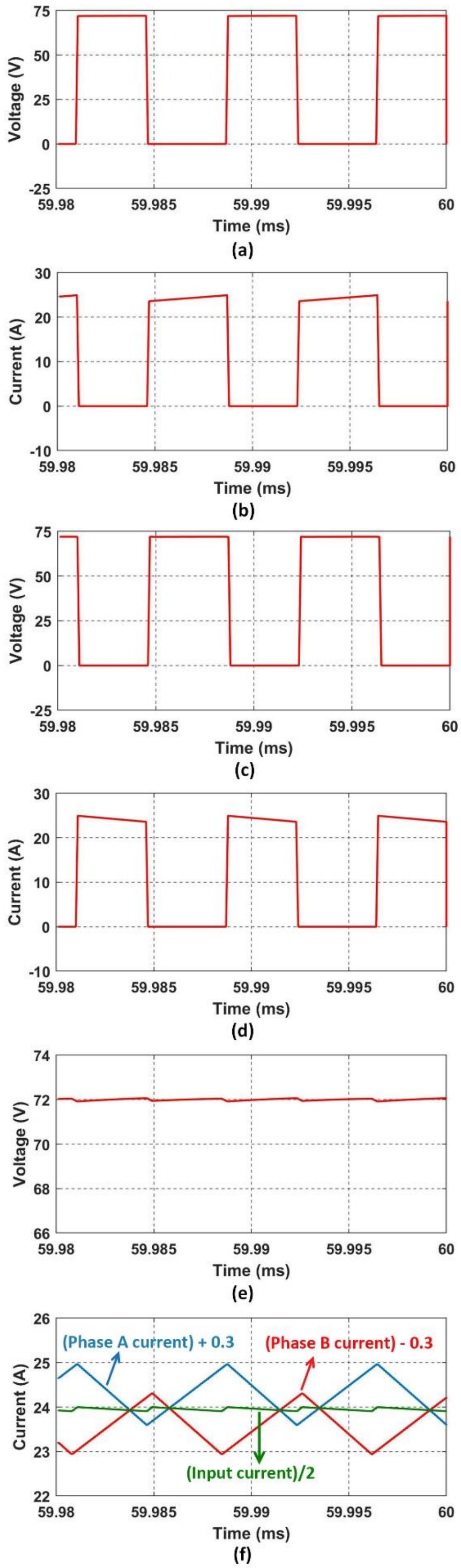

Fig. 11. Performance parameters waveforms for the designed two-phase boost converter: (a) switch voltage, (b) switch current, (c) diode voltage, (d) diode current, (e) output voltage, and (f) phases input current (in blue and red) and half of the converter input current (in green).

VII. Simulation and experimental results

A. Simulation results

The analytical results related to the design and operation of the selected two-phase boost converter should be validated using simulation results. For this purpose, the converter has been simulated in the PSIM software environment. The important performance waveforms of the designed two-phase boost converter are shown in Fig. 9 in rated load conditions (with 22.22 A output current). The maximum value of the switch voltage is 72.1 V and it has a 49 V RMS value (Fig. 9-a). In addition, the switch has a maximum current of 24.89 A and 17.7 A RMS value (Fig. 9-b). The maximum voltage and current values of the diode are 72 V (Fig. 9-c) and 24.9 A (Fig. 9-d), respectively. Obviously, the rated values of the selected switches and diodes are completely reasonable considering the simulation results. The converter has an output voltage with a 72.06 V average value and 0.22 V ripple voltage (Fig. 9-e), which are acceptable results considering the design goals. In addition, each phase has an input current with a 24.28 A average and 1.37 A ripple values (Fig. 9-f). However, the whole input current of the converter has an average of 47.9 A and a ripple of 0.19 A (Fig. 9-f), which is the result of using a two-phase structure. Note that in Fig. 9, half of the converter input current is presented simultaneously with the phases' input currents to show the current ripple cancellation effect of the two-phase structure. According to the simulation results, the designed converter satisfies the design requirements well.

B. Experimental results

The designed converter is implemented and connected to a DC source to extract the experimental test results. A lead-acid battery pack is used to simulate the reported fuel cell behavior considering its voltage-current profile presented in Fig. 1. Considering Table I, the fuel cell nominal operating voltage is simulated by the battery voltage value. An electronic load is used as the load for the fabricated two-phase boost converter. A circuit breaker is used to turn on/off the batteries. The set used for the required measurements is shown in Fig. 10. The experimental results for different parts of the converter are shown in Fig. 11. As can be seen, the MOSFET gate receives the switching command at a frequency of 130 kHz (Fig. 11-a). The switch voltages indicate correct MOSFET switching with the desired phase shift between two phases. The maximum stress voltage on the MOSFETs used in each phase is about 76.2 V (Fig. 11-b). As can be seen, due to the two-phase converter structure, the input current ripple has been reduced to 0.32 A (Fig. 11-d). As discussed in previous chapters, using 180 degrees of phase shift between two phases greatly reduces the total input current ripple of the converter and doubles the frequency of this ripple. The output voltage is stabilized at the desired value of 72.1 V and the voltage ripple is equal to 0.35 V (Fig. 11-e). The heatsink temperature is measured 33.3 ºC at its maximum. The same has been done for the switches, which are the hot spot of the converter, with the maximum temperature of 64.8 ºC. These results support the thermal performance of the converter. For evaluating the efficiency of the implemented prototype converter, its efficiency map is illustrated in Fig. 12. As can be seen, the converter has acceptable efficiency in different

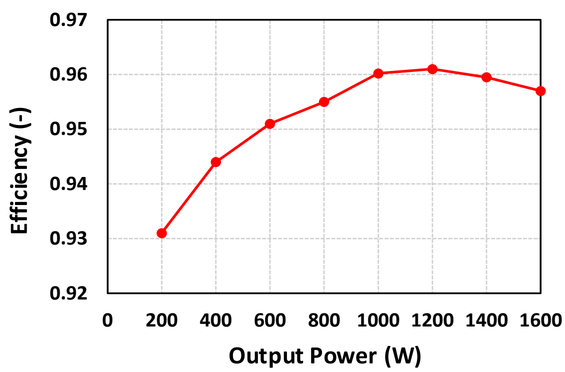

Fig. 12. Measured efficiency curve for the prototype converter.

loading conditions. According to the obtained experimental results, the accuracy of the theoretical results can be confirmed. On the other hand, these results are well-matched with the simulation results.

VIII. Conclusion

In this paper, a new study was done on the multi-phase DC-DC boost converters. The study proposed a solution to increase the power density and reliability of the boost converter for fuel cell applications because the fuel cell power systems usually require power electronics interfaces with high volumetric power density and high reliability. For this purpose, a different multi-phase boost converter was studied. According to the results presented for the main converter, using a two-phase structure, the capacitor and the input inductance volumes were reduced dramatically (67.1% and 86.4%, respectively) compared to the common single-phase structure. The reason for this reduction was using the phase shift angle between the switches command, which decreases the input current and output voltage ripples and doubles their frequency.

On the other hand, to study the converter reliability, some steps were taken in two operating conditions with and without input current ripple protection. The steps include calculation of the components' failure rates, reliability modelling (based on the Markov diagram), and ELL computation. Considering the results, the multi-phase structures from the most to the least reliable were the single-phase with ELL=0.1306pu, the two-phase with ELL=0.2271pu, and the four-phase with ELL=0.3434pu, respectively. In the end, the two-stage converter with a goal function (volume×ELL) of 0.0427 (which was 67.3% lower than the next best option) was selected as the best multi-layer configuration. The selected two-phase converter for fuel cell application was implemented, and the obtained experimental results verified the accuracy of the analytical results.

References

[1] Y. Ek, et al., "Tailoring Energy Efficiency for Urban Electric Buses: The GTECM Model for Enhanced Range and Sustainable Operation Using Real-Time Big Data", *IEEE Transactions on Intelligent Transportation Systems,* (Early Access), pp. 1-15, 2025, doi: 10.1109/TITS.2025.3558147.

[2] M. Vosoogh, et al., "Efficient Networked Microgrid Management Considering Plug-in Electric Vehicles and Storage Units", International Journal of Industrial Electronics, Control and Optimization, vol. 4, no. 2, pp. 245 –255, 2021, doi: 10.22111/ieco.2020.35847.1306.

[3] I. Denholm, et al., "Optimized Interleaved Ultra-High Gain DC-DC Power Converter With Low Ripple Input Current and Voltage Stress for Fuel Cell Systems", IEEE Access, vol. 12, no. 1, pp. 121052-121063, 2024, doi: 10.1109/ACCESS.2024.3450887.

[4] S. Sarani, et al., "An Isolated High Boost Ratio DC–DC Converter With Very Low Input Current Ripples", IEEE Transactions on Circuits and Systems, vol. 71, no. 9, pp. 4331–4335, 2024, doi: 10.1109/TCSII.2024.3386158.

[5] L. Qin, et al., "Transformer-Less Two-Phase Interleaved Boost Converter With Wide Input Voltage Range and Low Electric Stress for Fuel Cell Vehicles", IEEE Transactions on Power Electronics, vol. 40, no. 4, pp. 5480-5495, 2024, doi: 10.1109/TPEL.2024.3509524.

[6] A. Miremad, and S. Eren, "A Three-Level Current-Fed Dual-Active Bridge DC–DC Converter Under Dual Phase-Shift Control", IEEE Journal of Emerging and Selected Topics in Power Electronics, (Early Access), 2025, doi: 10.1109/JESTPE.2025.3561696.

[7] M. Benzine, et. al., "Experimental Validation of Fault-Tolerant Control With Signal-Based Diagnosis Approach for Interleaved Boost Converter in Fuel Cell Applications", IEEE Transactions on Power Electronics, vol. 40, no. 6, pp. 8592–8603, 2025, doi: 10.1109/TPEL.2024.3520876.

[8] R. Hazratian, et al., "An Improved Boost Topology According to the Voltage Lift Technique", International Journal of Industrial Electronics, Control and Optimization, Early access, 2025, doi: 10.22111/ieco.2025.50700.1652.

[9] N. Agrawal, et. al., "Optimal State Feedback-Integral Control of Fuel-Cell Integrated Boost Converter", IEEE Transactions on Circuits and Systems, vol. 69, no. 3, pp. 1382-1386, 2022, doi: 10.1109/TCSII.2021.3117716.

[10] G. Li, et. al., "A DC Voltage Robust Control Strategy of Boost Converter Based on Load Impedance and Input Voltage Observation", IEEE Transactions on Industrial Informatics, vol. 20, no. 5, pp. 7947-7956, 2024, doi: 10.1109/TII.2024.3367042.

[11] A. Mishra, et al., "Non-Linear Control of Interleaved Boost Converter Using Disturbance Observer-Based Approach", IEEE Access, vol. 13, no. 1, pp. 23833-23840, 2025, doi: 10.1109/ACCESS.2025.3537826.

[12] L. Fernandes, et al., "Multiphase Interleaved Boost Converter With Frequency Modulation for Sensorless Current Sharing", IEEE Transactions on Industrial Electronics, vol. 72, no. 6, pp. 5846-5856, 2025, doi: 10.1109/TIE.2024.3497341.

[13] V. Rao, and K. Sundaramoorthy, "Performance Analysis of Voltage Multiplier Coupled Cascaded Boost Converter With Solar PV Integration for DC Microgrid Application", IEEE Transactions on Industry Applications, vol. 59, no. 1, pp. 1013-1023, 2023, doi:10.1109/TIA.2022.3209616.

[14] K. C. Omran, and R. Beiranvand, “A High Step-Up Resonant Converter Based on Current-Fed Voltage Multiplier Technique”, IEEE Transactions on Industrial Electronics, vol. 71, no. 5, pp. 4562–4575, 2024, doi: 10.1109/TIE.2023.3283715.
[15] G. Wu, et. al., “Nonisolated high step-up DC–DC converters adopting switched-capacitor cell”, IEEE Transactions on Industrial Electronics, vol. 62, no. 1, pp. 383-393, 2015, doi: 10.1109/TIE.2014.2327000.
[16] P. Wang, et al., “Input-parallel output-series DC-DC boost converter with a wide input voltage range for fuel cell vehicles”, IEEE Transactions on Vehicular Technology, vol. 66, no. 9, pp. 7771-7781, 2017, doi: 10.1109/TVT.2017.2688324.
[17] Q. Li, et al., “An Improved Floating Interleaved Boost Converter With the Zero-Ripple Input Current for Fuel Cell Applications”, IEEE Transactions on Energy Conversion, vol. 34, no. 4, pp. 2167-2179, 2019, doi: 10.1109/TEC.2019.2936416.
[18] P. Azer, and A. Emadi, “Generalized State Space Average Model for Multi-Phase Interleaved Buck, Boost and Buck-Boost DC-DC Converters: Transient, Steady-State and Switching Dynamics', IEEE Access, vol. 8, no. 1, pp. 77735-77745, 2020, doi: 10.1109/ACCESS.2020.2987277.
[19] J. Gue, et al., “A Comprehensive Analysis for High-Power Density, High-Efficiency 60 kW Interleaved Boost Converter Design for Electrified Powertrains”, IEEE Transactions on Vehicular Technology, 2020, vol. 69, no. 7, pp. 7131-7145, 2020, doi: 10.1109/TVT.2020.2991395.
[20] B. Barry, et al., “Small-Signal Model of the Two-Phase Interleaved Coupled-Inductor Boost Converter”, IEEE Transactions on Power Electronics, vol. 33, no. 9, pp. 8052-8064, 2018, doi: 10.1109/TPEL.2017.2765920.
[21] E. Roshandel, et. al., “High Step-Up DC-DC Converter for Traction Drives Supplied by Fuel Cells”, 2019 IEEE Vehicle Power and Propulsion Conference (VPPC), 2019, doi: 10.1109/VPPC46532.2019.8952343.
[22] H. Tarzamni, et al., “Interleaved full ZVZCS DC–DC boost converter: analysis, design, reliability evaluations and experimental results”, IET Power Electronics, vol. 10, no. 7, pp. 835-845, 2017, doi: 10.1049/iet-pel.2016.0578.
[23] H. Tarzamni, et al., “Analysis and Reliability Evaluation of a High Step-Up Soft Switching Push–Pull DC–DC Converter”, IEEE Transactions on Reliability, vol. 69, no. 4, pp. 1376-1386, 2020, doi: 10.1109/TR.2019.2945413.
[24] H. Tarzamni, et al., “Comprehensive Analytics for Reliability Evaluation of Conventional Isolated Multiswitch PWM DC–DC Converters”, IEEE Transactions on Power Electronics, vol. 35, no. 5, pp. 5254-5266, 2020, doi: 10.1109/TPEL.2019.2944924.
[25] O. Alavi, et. al., “A Comparative Reliability Study of Three Fundamental Multilevel Inverters Using Two Different Approaches”, Electronics, vol. 5, no. 2, pp. 1-18, 2016, doi: 10.3390/electronics5020018.
[26] M. Radmehr and M. Mojibi, 'Reliability Assessment and Thermal Consideration of a Step-down DC/DC Converter', International Journal of Industrial Electronics, Control and Optimization, 2019, 2, (3), pp. 247-256 (doi: 10.22111/ieco.2019.25236.1042).
[27] US Department of Defense: “MIL-HDBK-217F (NOTICE 2), Military Handbook Reliability Prediction of Electronic Equipment”, Defense Technical Information Center, 1995, doi: 10.1109/RAMS.2010.5448046.
[28] A. Khosroshahi, et. al., “Reliability Evaluation of Conventional and Interleaved DC–DC Boost Converters”, IEEE Transactions on Power Electronics, vol. 30, no. 10, pp. 5821-5828, 2015, doi: 10.1109/TPEL.2014.2380829.
[29] S. V.Dhople, et al., “A Unified Approach to Reliability Assessment of Multiphase DC–DC Converters in Photovoltaic Energy Conversion Systems”, IEEE Transactions on Power Electronics, vol. 27, no. 2, pp. 739-751, 2012, doi: 10.1109/TPEL.2010.2103329.
[30] D. Zhou, et. al., “Mission Profile Based System-Level Reliability Analysis of DC/DC Converters for a Backup Power Application”, IEEE Transactions on Power Electronics, vol. 33, no. 9, pp. 8030-8039, 2018, doi: 10.1109/TPEL.2017.2769161.
[31] B.S. Dhillon, “Engineering Systems Reliability, Safety, And Maintenance”, CRC Press Taylor & Francis Group, 2017, doi: 10.1201/9781315160535.
[32] H. S. Chung, et. al. “Reliability of Power Electronic Converter Systems”, The Institution of Engineering and Technology, 2015, doi: 10.1049/PBPO080E.

Ghasem Rezazadeh received the B.Sc. degree in electrical engineering from Shahid Beheshti University, Tehran, Iran, in 2012, and the M.Sc. degree from Sharif University of Technology, Tehran, Iran, in 2014. He earned his Ph.D. degree through a joint supervision program between Sharif University of Technology and the University of Picardie Jules Verne, Amiens, France. He is currently an Assistant Professor at the University of Tehran, Tehran, Iran. His research interests include the design, modeling, and control of electric machines and power electronic converters.

Hossein Bagherian Farahabadi earned his B.Sc. and M.Sc. degrees in Electrical Engineering from Shahid Beheshti University, Iran, in 2010 and 2012, respectively, and completed his Ph.D. in Electrical Engineering at Malek Ashtar University of Technology, Iran, in 2017. He is currently serving as an Assistant Professor at Malek Ashtar University of Technology. His research interests encompass electric vehicle powertrains, power electronics, fuel cell technologies, and renewable energy systems.